

A deep look into the cores of young clusters[★]

I. σ -Orionis

H. Bouy^{1,2} **, N. Huélamo³, E. L. Martín^{1,4}, F. Marchis², D. Barrado y Navascués³, J. Kolb⁵, E. Marchetti⁵, M. G. Petr-Gotzens⁵, M. Sterzik⁶, V. D. Ivanov⁶, R. Köhler⁷, and D. Nürnberger⁶

¹ Instituto de Astrofísica de Canarias, C/ Vía Láctea s/n, E-38205 - La Laguna, Tenerife, Spain
e-mail: bouy@iac.es

² Astronomy Department, University of California, Berkeley, CA 94720, USA

³ Laboratorio de Astrofísica Espacial y Física Fundamental (LAEFF-INTA), PO BOX 78, E-28691, Villanueva de la Cañada, Madrid, Spain

⁴ University of Central Florida, Department of Physics, P.O. Box 162385, Orlando, FL 32816-2385, USA

⁵ European Southern Observatory, Karl Schwartzschild Str. 2, D-85748 Garching bei München, Germany

⁶ European Southern Observatory, Alonso de Cordova 3107, Vitacura, Casilla 19001, Santiago 19, Chile

⁷ ZAH, Landessternwarte, Königstuhl, D-69117 Heidelberg, Germany

Received ; accepted

ABSTRACT

Context. Nearby young clusters are privileged places to study the star formation history. Over the last decade, the σ -Orionis cluster has been a prime location for the study of young very low mass stars, substellar and isolated planetary mass objects and the determination of the initial mass function.

Aims. To extend previous studies of this association to its core, we searched for ultracool members and new multiple systems within the 1'5×1'5 central region of the cluster.

Methods. We obtained deep multi-conjugate adaptive optics (MCAO) images of the core of the σ -Orionis cluster with the prototype MCAO facility MAD at the VLT using the H and K_s filters. These images allow us to reach $\Delta H \approx 5$ mag as close as 0'2 on a typical source with H=14.5 mag. These images were complemented by archival SofI Ks-band images and *Spitzer* IRAC and MIPS mid-infrared images

Results. We report the detection of 2 new visual multiple systems, one being a candidate binary proplyd and the other one a low mass companion to the massive star σ Ori E. Of the 36 sources detected in the images, 25 have a H-band luminosity lower than the expected planetary mass limit for members, and H-K_s color consistent with the latest theoretical isochrones. Nine objects have additional *Spitzer* photometry and spectral energy distribution consistent with them being cluster members. One of them has a spectral energy distribution from H to 3.6 μ m consistent with that of a 5.5 M_{Jup} cluster member. Complementary NTT/SofI and *Spitzer* photometry allow us to confirm the nature and membership of two L-dwarf planetary mass candidates.

Key words. Instrumentation: Adaptive optics, Techniques: High Angular Resolution, Stars: visual binaries, Stars: Evolution, Stars: formation, Stars: general

1. Introduction

Over the last decade, the σ -Orionis cluster has become one of the prime locations for the study of brown dwarfs (BDs) and planetary-mass objects (PMOs). It is young (2–3 Myr), free of extinction ($A_V < 1$ mag) and it has a large low-mass population (Béjar et al., 1999, 2001; Barrado y Navascués et al., 2003; Béjar et al., 2004; Sherry et al., 2004; Kenyon et al., 2005; Caballero, 2007; Caballero et al., 2007; Caballero, 2008b; González-García et al., 2006; Sacco et al., 2008). The *Hipparcos* parallax to the central OB pair σ Ori AB is 320^{+120}_{-90} pc, and most previous studies used 350 pc to σ Ori AB

as the cluster distance. Other authors estimated distances at about 390 pc (Caballero, 2008a; Mayne & Naylor, 2008). Sherry et al. (2008) recently refined the measurement using main-sequence fitting and derived an improved value of 440 pc for a solar metallicity (Caballero, 2006). The cluster mass function rises steadily from the very low mass stars through the BDs and into the PMO domain (Béjar et al., 2001; Caballero et al., 2007). No obvious discontinuities are seen neither at the mass boundary between very low-mass stars and BDs nor at the frontier between BDs and PMOs, which is not surprising as the initial mass function does not have to know about the onset of nuclear reactions has occur during the subsequent evolution for stars and BDs. About two dozens PMOs candidates have been identified in the cluster (Zapatero Osorio et al., 2002, 2000; Caballero et al.,

Send offprint requests to: H. Bouy

* Observations made at the ESO La Silla and Paranal Observatory

** Marie Curie Outgoing International Fellow MOIF-CT-2005-8389

2007). About half of those have been confirmed spectroscopically (Martín et al., 2001; Barrado y Navascués et al., 2001; Martín & Osorio, 2003; Zapatero Osorio et al., 2000).

Evidences of disks were found around BDs and PMOs members from the detection of large H α emission, flux excesses at mid-infrared (mid-IR) wavelengths and large-amplitude photometric variability (Barrado y Navascués & Martín, 2003; Barrado y Navascués et al., 2003; Muzerolle et al., 2003; Caballero et al., 2006; Scholz & Eisloffel, 2004; Scholz & Jayawardhana, 2008; Hernández et al., 2007). In particular the very strong H α emission brown dwarf S Ori 71, located just above the cluster deuterium burning limit, displays excess flux in IRAC band 4.5 at 8.0 μ m (Caballero et al., 2007). If the cluster PMOs form in a similar way to the very low-mass stars and BDs, we expect that they would have dusty disks, probably of lower mass scaling with primary mass. Hernández et al. (2007) have recently suggested an increase of the disk frequency towards low masses in the cluster, with a peak of 40% in the mass interval 0.2–0.1 M_{\odot} . According to Caballero et al. (2007), the disk rate in the BD domain could be as high as 50%. Zapatero Osorio et al. (2007) and Scholz & Jayawardhana (2008) have reported mid-IR excesses in seven cluster PMOs, indicating that more than 30% of them have dusty disks. Gatti et al. (2008) reported that the mass accretion rate of σ -Orionis members harboring disks are significantly lower than that of e.g ρ -Oph members. On the other hand, Sacco et al. (2008) report a significantly larger fraction of accretors than in the neighboring λ -Orionis association where star formation might have been triggered by a supernova explosion (Dolan & Mathieu, 2001).

The multiplicity of σ -Orionis members has been devoted to a number of studies. Using a Fraunhofer micrometer, Struve (1837) resolved σ Ori AB for the first time as a close binary (0'26). A few decades later, Burnham (1893) used the micrometer mounted on the 36 inch telescope at the Lick Observatory and confirmed the multiplicity of σ Ori AB. Frost & Adams (1904) identified a possible spectroscopic component in the σ Ori AB binary system. More recently Caballero (2005) obtained adaptive optics (AO) images of the central region of the cluster, **resolving a number of sources**. Kenyon et al. (2005) used high resolution spectroscopic measurements of a sample of candidate very low-mass stars and BDs of the association to confirm the youth and membership and to search for spectroscopic binaries. Their preliminary conclusions, based on small-number statistics, shows that the binary fraction among σ -Orionis very low mass members is higher than that reported for their older field counterparts. Our understanding of the σ -Orionis cluster was recently complicated by the discovery by Jeffries et al. (2006); Sacco et al. (2007) of two distinct kinematics populations with different ages. However, most of the objects belonging to the older kinematic group are located northward from the central region of the σ -Orionis cluster, outside the area covered by the present study.

To extend the previous studies of σ -Orionis to its core we conducted an AO assisted imaging survey of the central part of the σ -Orionis cluster with the ESO multi-conjugated AO prototype instrument *Multi-Conjugate Adaptive Optics Demonstrator* (hereafter MAD Marchetti et al., 2006). These deep images have a resolution of $\approx 0'.1$ on a field of view of 1'5 \times 1'5.

2. MCAO Observations

2.1. MAD: a multi-conjugate adaptive optics facility at the VLT

MAD is a prototype instrument performing wide field-of-view, real-time correction for atmospheric turbulence (Marchetti et al., 2006). MAD was built by the European Southern Observatory (ESO) with the contribution of two external consortia to prove the feasibility of MCAO on the sky in the framework of the 2nd generation VLT instrumentation and of the European Extremely Large Telescope (ELT, Gilmozzi & Spyromilio, 2007). Originally designed as a laboratory experiment, MAD was offered to the community for science demonstration in November 2007 and January 2008 and installed at the Visitor Focus of the VLT telescope UT3 Melipal. An overview of its performances on the sky is given in Marchetti et al. (2007); Bouy et al. (2008). Its CAMCAO near-IR camera is based on a 2048 \times 2048 pixel HAWAII-2 infrared detector with a pixel scale of 0'.028 for a total field of view of 57'.3 \times 57'.3. At the time of the science demonstration observations, the CAMCAO camera suffered from a form of light leak. The amount of light and the pattern seen on the frames depend on the position of the camera, the DIT and the observing conditions, so that it is not possible to perfectly correct for it. The three wavefront sensors can close the loop on stars brighter than $V \approx 12$ mag within a circular area of 2' diameter.

2.2. Observations

During the on-sky demonstration run of MAD held in November 2007, a region of 1'5 \times 1'5 centered on the σ -Orionis cluster was observed in the H and K_s filters. Figure 1 gives an overview of the pointings and of the guide stars used for wavefront sensing. The geometrical distribution of the guide stars is quite asymmetric, leading to non-optimal corrections.

A set of NINT=30 images was obtained by dithering within a box of 15'' using the scanning capability of the infrared camera and keeping the adaptive-optics loop closed during the whole operation. The ambient conditions¹ during the observations reported by the ESO Ambient Conditions Database are given in Table 1. The conditions were significantly better during the H-band observations, with a coherence time of $\tau_0=3.2$ ms, and an average seeing of 0'.63 three times better than during the K_s band observations, explaining the better quality and sensitivity of the H band images. The exposure time per individual image was 30 \times 0.8 s (NDIT \times DIT), so that the total exposure time for the final mosaics added up to 12 min in each band.

The corresponding images were processed with the *Eclipse* reduction package (Devillard, 1997). They were first dark-subtracted and flat-fielded. The sky contribution was then removed from the input frameset by filtering out low-frequency sky variations from the cube of jittered images. The images were then aligned and stacked to produce the final mosaics. The astrometric solution was computed using isolated and unresolved 2MASS counterparts and is accurate to within 0'.1. The final processed mosaics are made available upon request from the authors of this article. Figure 2 shows the final H-band mosaic.

2.3. MCAO performances

The strehl ratio in the K_s band ranges from 2% to 6%. The undersampling of the PSF in the H band prevents us to compute

¹ At the zenith and in the visible.

meaningful strehl ratios, but the performances are expected to be similar. The quality of the correction follows closely the geometry of the 3 reference stars, and most sources away from the line made by the 3 reference stars are elongated with ellipticities in the range $0.41 \leq e \leq 0.95$. In spite of the low strehl ratios, the PSFs are much sharper than in the seeing limited SofI images (full width at half maximum FWHM $\approx 0''.8$, see Section 3.1) with an average FWHM of $0''.10$ in H and $0''.15$ in K_s .

Adaptive-optics provide not only high spatial resolution but also high-contrast images. To illustrate the performances of the instrument and the limitations of the observations, we computed the limit of sensitivity for two cases: a star with H & $K_s=14.5$ mag located in a region of good AO correction (hereafter referred to “center”) and a fainter star (H=15.88 mag, $K_s=15.55$ mag) located in a region of worse AO correction (hereafter referred to “edge”). The limit of sensitivity was computed using the $3\text{-}\sigma$ standard deviation of the PSF radial profile. Figure 3 shows the results. The MAD images allow detection with a magnitude contrast $\Delta m=4$ mag at $0''.25$ and $0''.35$ in H and K_s , respectively on a 14.5 mag star at the center. Sources brighter than ≈ 8 mag were saturated or above the detector linearity limit. We detected sources as faint as $K_s=19.55$ mag and H=21.65 mag ($3\text{-}\sigma$ detection), therefore well below the deuterium burning limit at the age (1–5 Myr) and distance (440 pc) of the cluster (predicted at H=17.03 mag for the DUSTY models and H=16.87 mag for the COND models, Chabrier et al., 2000; Baraffe et al., 2003).

2.4. Photometry

Because of the complexity of the MCAO wavefront sensing, the PSF shows spatial variations due to anisoplanetic effects in the AO observations that can affect PSF photometry. To alleviate this problem, we took advantage of the sparsity of the field and performed aperture photometry rather than PSF fitting, except in a few cases of close multiple systems or when the source was located in the halo of a bright neighboring massive star. In these latter cases we extracted the photometry using nearby isolated stars as reference PSF. The aperture photometry was performed using standard routines with the *daophot* package within IRAF², using an aperture of 18 pixels ($0''.5$), and a sky annulus between 20–24 pixels ($0''.56\text{--}0''.67$). Two well-behaved isolated and unresolved 2MASS sources with clean H-band photometry (quality flag A, 2MASS J05384652-0235479 and 2MASS J05384746+0235252) were used to derive the photometric instrumental zeropoints given in Table 2. The K_s -band zeropoints were computed using 11 clean and unresolved matches found in the SofI image (see Section 3.1). Some systematic errors might remain because of the strong anisoplanetism and unaccounted color terms. They are difficult to estimate because of the small number of well behaved counterparts in the 2MASS and SofI catalogs. The relatively small scatter between the MAD K_s and SofI K_s photometry of the 11 isolated sources in common (well within the uncertainties) suggest that the aperture was chosen large enough that these spatial variations do not affect the final photometry too much. The 36 detected sources and their photometry are reported in Table 3.

² IRAF is distributed by the National Optical Astronomy Observatory, which is operated by the Association of Universities for Research in Astronomy (AURA) under cooperative agreement with the National Science Foundation.

3. Complementary archival data

We searched the *ESO* and *Spitzer* public archives for complementary datasets of the same field.

3.1. NTT/SofI images:

The cluster had been observed in the K_s band with SofI at the NTT on 2001 December 12 (P.I. Testi, Programme 67.C-0042). A set of NINT=15 dithered images of 12×5 s (NDIT×DIT) was obtained that night. We retrieved the data and the corresponding calibration frames and processed them following standard procedures using the recommended *Eclipse* reduction package. The seeing (measured on the image) was $0''.8$. We extracted the PSF photometry of all the sources brighter than the $3\text{-}\sigma$ noise of the local background using Diolaiti et al. (2000) Starfinder code. Using six well behaved (quality flag A) unresolved 2MASS sources we derive a zeropoint magnitude of 23.96 ± 0.19 mag. The catalogue is available in electronic form. The limit of detection of the images is ≈ 20 mag, and the limit of completeness is ≈ 19 mag as illustrated in Fig. 4. On the bright side, the detector non-linearity reaches about 3% at 14000 A.D.U., corresponding to $K_s=13.6$ mag.

3.2. VLT/NACO images:

The central stars σ Ori AB and D have been observed twice with the AO facility NACO on the VLT (Programs 074.C-0084 and 074.C-0628, P.I. Neuhäuser). A first set of 4 images of 100×0.345 s (NDIT×DIT) each was obtained on 2004 October 10 in the K_s band with the S13 camera. A second set of 10 dithered images of 10×0.345 s (NDIT×DIT) was obtained in the narrow band Bry (NB_2.17) filter. We retrieved the data and the associated calibration frames and processed them using the recommended *Eclipse* reduction package. The second epoch narrow band images are much shallower than the first ones, and we do not discuss them further. The limited number of images obtained at the first epoch does not allow to correct perfectly for the bad and hot pixels. The brightness of the massive OB pair makes it an easy target for NACO and the strehl ratio was high (60–65%, FWHM= $0''.07$). The final image is shown in Fig. 5

3.3. Spitzer data

The σ -Orionis cluster was observed with *Spitzer* IRAC on 2004 October 08 in the course of program 37 (P.I. Fazio, Hernández et al., 2007) and with IRAC on 2007 April 03 in the course of program 30395 (P.I. Scholz, Scholz & Jayawardhana, 2008). Program 37 was executed in High Dynamic Range (HDR) mode providing equal numbers of consecutive short and long exposures. Table 4 gives a summary of the observations. We retrieved the calibrated, individual IRAC BCD (Basic Calibrated Data) images and stacked them following the procedures recommended by the Spitzer Science Center (SSC) with the MOPEX software package and the relevant calibration files. The final long exposure mosaics in channel 1 and 3 are made of images of both programs 37 and 30395 weighted by their exposure times. Program 30395 channel 2 and 4 images do not overlap with our area of interest. The final mosaic images in these 2 bands are therefore made of program 37 images only. The short exposure mosaics allowed us to extract the photometry of bright sources otherwise saturated in the long exposure mosaics. A total of 9 sources detected in the MAD images are also detected in one (or more) *Spitzer* IRAC band. We extracted the photometry us-

ing standard PSF photometry procedures within the Interactive Data Language. Uncertainties were tentatively estimated from the Poisson noise weighted by the coverage maps of the mosaics, but the presence of the bright and asymmetric halo and ghosts around the massive stars make it difficult to estimate reliable uncertainties. The results are given in Table 5 and Fig. 6. The cluster was also observed with MIPS on 2004 March 17 in the course of Program 58 (P.I. Rieke). These observations are described in details in Hernández et al. (2007). Except for one object (described in Section 7), the coarser resolution and lesser sensitivity of the MIPS images in the vicinity of the massive central OB stars does not allow us to extract any useful MIPS photometry for the MAD sources.

4. Nature of the detections

In order to rule out the possibility that some of the faint sources detected in the MAD images are artefacts (such as e.g bad pixels, remnants, ghosts, cosmic ray events, etc.), we compare the SofI, NACO and MAD images. Only seven objects detected in the MAD H-band image are not detected in the MAD and SofI K_s -band images, ruling out the possibility of artefacts for the other 29 objects.

Two of these seven sources without K_s band counterparts in either the MAD or SofI images fall within the field of view of the NACO K_s image. Only one is detected (SigOri-MAD-11, see Fig. 5 and discussion hereafter). The other one (SigOri-MAD-13) falls in an area of the NACO mosaic where only one image was co-added (no overlap with the other 3 images) and where the sensitivity is therefore significantly worse. It is not detected in the SofI image as it falls on a diffraction spike of the bright OB stars where the limit of sensitivity is significantly worse. We estimate the limit of sensitivity at the expected position of SigOri-MAD-13 in both the NACO and SofI images by adding artificial stars of decreasing luminosity until the $3\text{-}\sigma$ detection algorithm misses it. The detection limits measured that way are $K_s \approx 17$ mag in both the NACO and SofI image, thus just at the limit to detect SigOri-MAD-13. The nature of SigOri-MAD-13 is therefore uncertain and must be confirmed with new images.

The five remaining H-band sources without MAD, SofI or NACO K_s counterpart are either located on diffraction spikes, or in a region where the halos of the bright massive stars are strong, degrading the limit of sensitivity of the SofI or NACO images. These five sources are the faintest of our sample, and in the state of the currently available data we can not rule out the possibility that they are false positives. However, the presence of confirmed sources with similar magnitudes (e.g SigOri-MAD-26) in both the H and K_s images and the quality of the correlation between the PSF of these sources and the PSF of nearby objects (all better than 0.78) suggest that these detections are likely to be real as well. New images with a better signal-to-noise ratio are required to confirm their nature. An upper limit on their K_s band luminosity was derived by adding artificial stars of decreasing luminosity at the expected position of the source until the $3\text{-}\sigma$ detection algorithm misses it.

SigOri-MAD-27 falls close to the position of a saturated bright massive star's remnant spot in both the H and K_s MAD image (see Fig. 2). The associated H band photometry is therefore unreliable and should be considered with caution. The K_s band photometry was measured in the SofI image and is therefore unaffected and reliable.

5. Multiple systems

With an average resolution of $\approx 0''.1$, the MAD images resolve a number of multiple systems.

5.1. Previously known multiple systems

σ Ori AB: The brightest star in σ -Orionis, which gives its name to the cluster, is a known multiple system made of at least two components, σ Ori A and B (Struve, 1837). The pair is saturated in all the MAD, NACO K_s and SofI images and no useful broad-band photometry can be performed. We used the unsaturated NACO Bry image to measure the relative astrometry of the pair, as reported in Table 7.

σ Ori AD: (Struve, 1837) The two stars are heavily saturated in the MAD image. σ Ori A is saturated in the NACO image, but not σ Ori D. The D component is outside the field of view of the unsaturated NACO Bry image. The saturation of the NACO broad-band K_s image is not as bad as in the MAD images and a careful fit of the wings of the saturated PSF of σ -Ori A and its Airy rings allow us to measure the relative astrometry of the AD pair.

σ Ori C: has been resolved as a wide binary by Caballero (2005). It is clearly resolved in the new MAD images. The primary σ Ori Ca is saturated in the MAD H-band but the large separation allows us to measure accurately the photometry of Cb. From the unresolved 2MASS photometry, we derive the relative H-band photometry given in Table 7. It is also resolved in the SofI image but the bright Ca primary is saturated.

5.2. New multiple systems

σ Ori IRS1: the x-ray, radio, mid- and near-infrared source (Skinner et al., 2008; van Loon & Oliveira, 2003; Sanz-Forcada et al., 2004; Caballero, 2005; Drake, 1990) is resolved in both the MAD and NACO images and we measure accurate relative astrometry and photometry (see Table 7). The resolved photometry and colors of the individual component correspond, according to the latest NextGen models of Baraffe et al. (1998), to masses of $0.47 M_{\odot}$ and $0.12 M_{\odot}$, but these values must be considered with caution as previous studies reported a high local extinction toward this source. The object was recently resolved independently by Caballero & Rebolo (in prep., private communication), and detected with AO in the optical but unresolved by Turner et al. (2008). van Loon & Oliveira (2003) detected this object in the mid-IR with TIMM12 at the ESO/3.6m and associated it to the radio source reported at 2, 6 and 20 cm by Drake (1990) and to the mid-IR source IRAS 05362-0237. Based on the mid-IR excess, the displacement between the mid-IR photocenter (associated to a disk) and radio photocenter (associated to free-free emission from an ionization front) and the presence of processed silicate grains revealed in their mid-IR spectrum, they describe the object as a proplyd, a proto-planetary disk being dispersed by the intense ultraviolet (UV) radiation from σ Ori AB (O'Dell & Wong, 1996). The source was marginally resolved in their $8.6 \mu\text{m}$ images, with a size of $\approx 1''.1$. Skinner et al. (2008) high resolution Chandra xray observations show that the xray source associated to σ Ori IRS1 is variable and must be a magnetically-active young T Tauri star. To further investigate the nature of this source, we retrieved MIPS images of the cluster from the *Spitzer* public archive. The observations are

described in details in Hernández et al. (2007). The central massive pair σ Ori AB is saturated in all IRAC and MIPS 24 μm images preventing us to extract useful photometry for σ Ori IRS1. A bright source is detected in the MIPS 70 μm image at $\alpha = 05^{\text{h}}38^{\text{m}}44.9^{\text{s}}$ and $\delta = -02^{\circ}35'56.0''$, i.e. only $2''.24$ from σ Ori IRS1 but $4''.9$ from σ Ori AB. With a FWHM of $\approx 21''.5$, it is difficult to associate the mid-IR source to any of these two objects with certainty, but the closer distance to the MAD, TIMMI-2 and VLA sources (see Fig. 10) and the expected much lower 70 μm flux of the massive pair lead us to associate the MIPS 70 μm source to σ Ori IRS1. Using PSF photometry, we measure a flux of 752 ± 150 mJy. This value is not consistent with the IRAS 60 μm photometry given for the associated source IRAS 05362-0237, which is 6.95 Jy. With a much broader PSF, the IRAS photometry includes the flux of nearby bright nebulosities and is therefore unreliable. Fig. 10 shows the relative positions of the MAD, VLA, TIMMI-2 and *Spitzer* detection as well as the spectral energy distribution of the source. The formation and evolution of such a system in a Trapezium-like cluster at a projected distance of only ≈ 1200 AU (the physical distance might be much larger) of a pair of massive OB stars make it particularly interesting. One can indeed wonder how such a pair and its circum-binary disk has survived the dynamical interactions commonly happening in such a cluster for as long as 1–3 Myr. If confirmed, the nature of this low-mass/very low mass pair will provide a direct proof that relatively wide (>100 AU) low mass pairs and their disk can survive the gravitational interactions and the photo-evaporation in the early stages of the formation of proto-stellar clusters.

σ Ori E: is resolved in the MAD images. The two components are saturated in the H-band image. The secondary is not saturated in the K_s -band image, but the heavy saturation of the primary and its halo prevent us to make any accurate measurement of the photometry of the secondary. Table 7 gives approximate measurements of the separation and position angle. We tentatively derive an upper limit on the K_s -band luminosity of the companion by adding artificial PSF of increasing luminosity at its diametrically opposed position until the luminosity matches that of the companion. The luminosity roughly estimated this way ($K_s \approx 10\text{--}11$ mag) corresponds to an estimated mass of $0.4\text{--}0.8 M_{\odot}$. σ Ori E was suspected to have a low mass companion for several decades. Walborn (1974) had noticed a peculiar variable $H\alpha$ emission in σ Ori E spectrum and interpreted it (among other hypothesis) as the effect of the possible presence of a very low mass companion. Using *uvby* beta light curves, Hesser et al. (1976) later suggested that σ Ori E was indeed a binary system, and put an upper limit on the mass of the companion at $M < 0.1 M_{\odot}$ for inclination $i > 45^{\circ}$. The source displayed repeated xray flares (reported with *ROSAT*, *XMM-Newton* and *Chandra*, respectively by Groote & Schmitt, 2004; Sanz-Forcada et al., 2004; Skinner et al., 2008). The xray activity was suspected by several of these authors to be in part due to the presence of an unseen low mass companion. The MAD images show that a low mass companion is indeed present next to the massive helium-strong σ Ori E star and could be responsible for the observed xray activity.

6. Substellar and isolated planetary mass candidates

Fig. 8 shows a color-magnitude diagram of all the sources detected in the MAD images, as well as catalogs of cluster members from the literature for comparison. A number of

sources have luminosities and colors consistent with the cluster isochrones and with substellar and planetary masses. With only two bands and no comparison field away from the cluster it is difficult to assess the level of contamination. Using the model of stellar population synthesis of the Galaxy of Robin et al. (2003) we find that the expected contamination by background giants or foreground dwarfs in the field of view of the MAD images must be very low. Caballero et al. (2008) recently estimated that the number of expected field L and T-dwarf contaminants toward the cluster adds up to ≈ 550 objects per 1 deg^2 , corresponding to < 0.4 contaminant in the case of our study. The contamination by extragalactic sources is expected to be much higher, as illustrated by the recent survey of the cluster by Hernández et al. (2007). In the current state of the data, it is not possible to estimate the contamination by extragalactic sources among the MAD detections. We nevertheless note that none of the sources identified in the MAD images is extended while most extragalactic sources rejected by Hernández et al. (2007) in their analysis were extended. Additional observations are required to confirm the membership of the new candidates.

Using the *Spitzer* photometry, we tentatively assess further the nature of the nine sources with mid-IR counterparts. Figure 6 shows the spectral energy distributions (SED) of the stellar candidate members. All but SigOri-MAD-34 match very well the median SED of cluster members measured by Hernández et al. (2007), ruling out the possibility of extragalactic contaminants. SigOri-MAD-34 displays mid-IR excess most likely related to a circumstellar disk and providing further evidence of its youth and membership to the association. Figure 7 shows the SEDs of all the MAD substellar candidates with a *Spitzer* counterpart. All but SigOri-MAD-31 match also very well the median SED of cluster members and the synthetic DUSTY SEDs of the corresponding H-band luminosity at the exact distance of the cluster sequence (440 pc, Sherry et al., 2008) and for an age of 1 Myr. These SEDs could be equally well fitted by foreground late-M field dwarf at a distance of ≈ 100 pc, preventing us to draw any firm conclusion regarding their membership to the association. Spectroscopy and proper motion measurements are required to confirm their nature. SigOri-MAD-6 (2MASS J05384454-0235349) was suggested to be a background A-F star or an extragalactic source by Caballero (2007) based on its blue J- K_s color. The new 3.6 μm photometric measurement allows us to rule out the extragalactic contaminant hypothesis. The J-band photometric measurement reported by Caballero (2007) is ≈ 0.7 mag brighter than the expected J-band luminosity of a $0.025 M_{\odot}$ cluster member. All the other measurements (H, K_s and 3.6 μm) are in good agreement with the luminosities expected for a $0.025 M_{\odot}$ cluster member as shown in Fig. 7. The J-band luminosity discrepancy could be due to underestimated errors on the photometric measurement in the proximity of the bright central OB pair (Caballero, private communication). Until new J-band measurements are obtained, SigOri-MAD-6 remains a good brown dwarf member candidate.

Mayrit 72345 and Mayrit 111335 are two L-dwarf candidate members reported by Caballero (2007) using optical, near-infrared and xray photometry. The two sources are detected in the SofI K_s -band image and in the *Spitzer* IRAC1, 2 and 3 channels (respectively SigOri-SofI-181 and SigOri-SofI-142, Table 6 and 8). The SofI photometry is in good agreement with Caballero (2007) photometry within the uncertainties. Their SEDs, shown in Fig. 9, allows us to rule out the possibility that these two sources are extragalactic contaminants. They are inconsistent with a purely photospheric emission and display some excess in the near- and mid-IR most likely related to

the presence of circumstellar material, assessing their youth and membership to the association. In the near-IR, these two objects look like lower luminosity analogues of the substellar member S Ori J053902.1-023501 (Caballero et al., 2007). Their mid-IR excess is less than that reported for S Ori J053902.1-023501. Caballero (2007) associated Mayrit 72345 to the xray source NX 77 detected with *XMM-Newton* by Franciosini et al. (2006). Figure 6 shows that their SEDs is very similar to that of SigOri-MAD-31, adding further evidence that this latter source is likely to be a very low mass substellar member. The **J and H-band luminosities of these 3 objects are well matched by a DUSTY SED with a mass of $\approx 5.5 M_{\text{Jup}}$ at a distance of 440 pc and at an age of 1 Myr (Fig. 6 and 7). At 5 Myr, these luminosities correspond to a mass of $\approx 7 M_{\text{Jup}}$, as described in Caballero (2007).** This estimate is only tentative as the objects display some near-IR excess.

7. Notes on individual targets

SigOri-MAD-11: is detected in the MAD ($12\text{-}\sigma$) and NACO ($3\text{-}\sigma$) images, confirming that it is a real detection. The two observations are separated by ≈ 3 yr and we tried to measure the proper motion relative to the closest unsaturated object σ Ori IRS1a. The large uncertainties (dominated by the poorly calibrated camera distortions, of the order of 1% of the pixel scale for CONICA and unknown for CAMCAO see e.g. Seifahrt et al., 2007; Eggenberger et al., 2007) and the small proper motion of the association (only ≈ 6 mas/yr, corresponding to ≈ 18 mas between the two epochs, or 1.35 CONICA pixel and 0.9 CAMCAO pixel) make these measurements inconclusive. New measurements covering a larger timescale will be required to confirmed that this source is co-moving with the nearby massive cluster members.

SigOri-MAD-26: is the faintest and reddest object with a detection in both H and K_s . It has a counterpart in the SofI image. Its luminosity and color are consistent with the DUSTY 1 Myr isochrone at 440 pc within the uncertainties, but largely inconsistent with the color of the confirmed member S Ori 70, which lies on the much bluer COND isochrones. This source is therefore unlikely to be a very low mass substellar member of the association. The K-band peak in the SED could be that of a low redshift ($z \approx 0.5$) galaxy. We nevertheless note that an average size galaxy (10 000 light year diameter) at that distance would have been easily resolved by our MCAO images. **The object lies in the direction of the reddening vector, suggesting that it is most likely an extincted source.**

SigOri-MAD-34: (*Mayrit 53049*) is clearly detected in all IRAC four bands, and displays some excess at long wavelength indicating the presence of circumstellar material and adding further evidence that the object is young and member of the association. Assuming an age of 1 Myr and a distance of 440 pc, its H and K_s -band luminosities correspond to a mass of $\approx 0.45 M_{\odot}$ according to the NextGen models.

8. Spatial distribution of BD and PMOs

Using DENIS, 2MASS and previously published catalogs, Caballero (2008b, 2007) recently concluded that there is an apparent deficit of very low mass stars and high-mass BDs in the

central $4'$ of the cluster. The relatively large number of faint objects detected in our new images of the central part of the cluster suggest that a large fraction of very low mass members might have been missed by the previous survey because of the dazzling central massive stars. Their presence affected all the previous seeing limited observations making the detection of very low-mass cluster members in this region very difficult, if not impossible. The unprecedented dynamic range provided by MAD allows us to detect a number of faint sources that, if confirmed as cluster members, could fill the very low mass end of the central cluster population. Additional observations are required to confirm the membership and nature of the candidates and provide a quantitative answer to that question.

9. Conclusions and future prospects

Using multi-conjugate AO images of the core of the σ -Orionis cluster, we have identified 6 new BD candidates and 25 planetary mass candidates. Five of these have additional mid-IR *Spitzer* IRAC photometry consistent with that of sub-stellar members. In the current state of the data, it is not possible to conclude on their membership to the association as they could also be foreground late-M dwarfs. The candidate proplyd σ Ori IRS1 is resolved as a binary. The high spatial resolution MAD images resolve 5 pairs, including 2 previously unknown ones. The results presented in this paper illustrate the capacity of multi-conjugate AO to probe the immediate vicinity of young massive OB stars in great details. Using complementary archival SofI and *Spitzer* images, we were able to confirm the membership of two L-dwarf candidate members that exhibit near- and mid-IR excess associated to a disk. One planetary mass candidate newly detected in the MAD images (*SigOri-MAD-31*) displays a SED very similar to these latter two, suggesting that it is also a L-dwarf member of the association harboring a disk. The presence or absence of very low mass stars, BDs and planetary mass objects close to massive stars provides novel constraints on the models of formation. Follow-up observations of the candidates are very much needed to confirm the nature and membership of the new candidates, and quantitative feedback on the models of formation.

Acknowledgements. The authors are grateful to Paola Amico for her support at ESO. We thank J. A. Caballero and V. Béjar for fruitful discussions, suggestions and comments on the manuscript. We thank our anonymous referee for her/his review of the manuscript. H. Bouy acknowledges the funding from the European Commission's Sixth Framework Program as a Marie Curie Outgoing International Fellow (MOIF-CT-2005-8389). F. Marchis work was supported by the National Science Foundation Science and Technology Center for Adaptive Optics, and managed by the University of California at Santa Cruz under cooperative agreement No AST-9876783. Nuria Huélamo and David Barrado y Navascués are funded by Spanish grants MEC/ESP2007-65475-C02-02, MEC/Consolider-CSD2006-0070 and CAM/PRICIT-S-0505/ESP/0361. This work is based on observations obtained with the MCAO Demonstrator (MAD) at the VLT (ESO Public data release), which is operated by the European Southern Observatory. The MAD project is led and developed by ESO with the collaboration of the INAF-Osservatorio Astronomico di Padova (INAF-OAPD) and the Faculdade de Ciências de Universidade de Lisboa (FCUL). Based on observations made with ESO Telescopes at the La Silla or Paranal Observatories under programmes 67.C-0042, 074.C-0084, and 074.C-0628. This publication makes use of data products from the Two Micron All Sky Survey, which is a joint project of the University of Massachusetts and the Infrared Processing and Analysis Center/California Institute of Technology, funded by the National Aeronautics and Space Administration and the National Science Foundation. This work has made use of the Vizier Service provided by the Centre de Données Astronomiques de Strasbourg, France (Ochsenbein et al., 2000). This research used the facilities of the Canadian Astronomy Data Centre operated by the National Research Council of Canada with the support of the Canadian Space Agency.

References

- Baraffe, I., Chabrier, G., Allard, F., & Hauschildt, P. H. 1998, *A&A*, 337, 403
- Baraffe, I., Chabrier, G., Barman, T. S., Allard, F., & Hauschildt, P. H. 2003, *A&A*, 402, 701
- Barrado y Navascués, D., Béjar, V. J. S., Mundt, R., et al. 2003, *A&A*, 404, 171
- Barrado y Navascués, D. & Martín, E. L. 2003, *AJ*, 126, 2997
- Barrado y Navascués, D., Zapatero Osorio, M. R., Béjar, V. J. S., et al. 2001, *A&A*, 377, L9
- Béjar, V. J. S., Caballero, J. A., Rebolo, R., Zapatero Osorio, M. R., & Y Navascués, D. B. 2004, *Ap&SS*, 292, 339
- Béjar, V. J. S., Martín, E. L., Zapatero Osorio, M. R., et al. 2001, *ApJ*, 556, 830
- Béjar, V. J. S., Zapatero Osorio, M. R., & Rebolo, R. 1999, *ApJ*, 521, 671
- Bouy, H., Kolb, J., Marchetti, E., et al. 2008, *A&A*, 477, 681
- Burnham, S. W. 1893, *Astronomische Nachrichten*, 131, 329
- Caballero, J. A. 2005, *Astronomische Nachrichten*, 326, 1007
- Caballero, J. A. 2006, PhD thesis, PhD thesis, Universidad de La Laguna, Spain (2006)
- Caballero, J. A. 2007, *Astronomische Nachrichten*, 328, 917
- Caballero, J. A. 2008a, *MNRAS*, 383, 750
- Caballero, J. A. 2008b, *MNRAS*, 383, 375
- Caballero, J. A. 2008c, *A&A*, 478, 667
- Caballero, J. A., Béjar, V. J. S., Rebolo, R., et al. 2007, *A&A*, 470, 903
- Caballero, J. A., Burgasser, A. J., & Klement, R. 2008, *A&A*, 488, 181
- Caballero, J. A., Martín, E. L., Zapatero Osorio, M. R., et al. 2006, *A&A*, 445, 143
- Chabrier, G., Baraffe, I., Allard, F., & Hauschildt, P. 2000, *ApJ*, 542, 464
- Devillard, N. 1997, *The Messenger*, 87, 19
- Diolaiti, E., Bendinelli, O., Bonaccini, D., et al. 2000, in Presented at the Society of Photo-Optical Instrumentation Engineers (SPIE) Conference, Vol. 4007, Proc. SPIE Vol. 4007, p. 879-888, Adaptive Optical Systems Technology, Peter L. Wizinowich; Ed., ed. P. L. Wizinowich, 879-888
- Dolan, C. J. & Mathieu, R. D. 2001, *AJ*, 121, 2124
- Drake, S. A. 1990, *AJ*, 100, 572
- Eggenberger, A., Udry, S., Chauvin, G., et al. 2007, *A&A*, 474, 273
- Franciosini, E., Pallavicini, R., & Sanz-Forcada, J. 2006, *A&A*, 446, 501
- Frost, E. B. & Adams, W. S. 1904, *ApJ*, 19, 151
- Gatti, T., Natta, A., Randich, S., Testi, L., & Sacco, G. 2008, *A&A*, 481, 423
- Gilmozzi, R. & Spyromilio, J. 2007, *The Messenger*, 127, 11
- González-García, B. M., Zapatero Osorio, M. R., Béjar, V. J. S., et al. 2006, *A&A*, 460, 799
- Groote, D. & Schmitt, J. H. M. M. 2004, *A&A*, 418, 235
- Hernández, J., Hartmann, L., Megeath, T., et al. 2007, *ApJ*, 662, 1067
- Hesser, J. E., Walborn, N. R., & Ugarte, P. P. 1976, *Nature*, 262, 116
- Jeffries, R. D., Maxted, P. F. L., Oliveira, J. M., & Naylor, T. 2006, *MNRAS*, 371, L6
- Kenyon, M. J., Jeffries, R. D., Naylor, T., Oliveira, J. M., & Maxted, P. F. L. 2005, *MNRAS*, 356, 89
- Marchetti, E., Brast, R., Delabre, B., et al. 2006, in Presented at the Society of Photo-Optical Instrumentation Engineers (SPIE) Conference, Vol. 6272, Advances in Adaptive Optics II. Edited by Ellerbroek, Brent L.; Bonaccini Calia, Domenico. Proceedings of the SPIE, Volume 6272, pp. 627200 (2006).
- Marchetti, E., Brast, R., Delabre, B., et al. 2007, *The Messenger*, 129, 8
- Martín, E. L. & Osorio, M. R. Z. 2003, *ApJ*, 593, L113
- Martín, E. L., Zapatero Osorio, M. R., Barrado y Navascués, D., Béjar, V. J. S., & Rebolo, R. 2001, *ApJ*, 558, L117
- Mayne, N. J. & Naylor, T. 2008, *MNRAS*, 386, 261
- Muzerolle, J., Hillenbrand, L., Calvet, N., Briceño, C., & Hartmann, L. 2003, *ApJ*, 592, 266
- Ochsenbein, F., Bauer, P., & Marcout, J. 2000, *A&AS*, 143, 23
- O'Dell, C. R. & Wong, K. 1996, *AJ*, 111, 846
- Patten, B. M., Stauffer, J. R., Burrows, A., et al. 2006, *ApJ*, 651, 502
- Robin, A. C., Reylé, C., Derrière, S., & Picaud, S. 2003, *A&A*, 409, 523
- Sacco, G. G., Franciosini, E., Randich, S., & Pallavicini, R. 2008, *ArXiv e-prints*, 805
- Sacco, G. G., Randich, S., Franciosini, E., Pallavicini, R., & Palla, F. 2007, *A&A*, 462, L23
- Sanz-Forcada, J., Franciosini, E., & Pallavicini, R. 2004, *A&A*, 421, 715
- Scholz, A. & Eislöffel, J. 2004, *A&A*, 419, 249
- Scholz, A. & Jayawardhana, R. 2008, *ApJ*, 672, L49
- Seifahrt, A., Roell, T., & Neuhauser, R. 2007, *ArXiv e-prints*, 706
- Sherry, W. H., Walter, F. M., & Wolk, S. J. 2004, *AJ*, 128, 2316
- Sherry, W. H., Walter, F. M., Wolk, S. J., & Adams, N. R. 2008, *AJ*, 135, 1616
- Skinner, S. L., Sokal, K. R., Cohen, D. H., et al. 2008, *ArXiv e-prints*, 805
- Skrutskie, M. F., Cutri, R. M., Stiening, R., et al. 2006, *AJ*, 131, 1163
- Struve, F. G. W. 1837, *Astronomische Nachrichten*, 14, 249
- Turner, N. H., ten Brummelaar, T. A., Roberts, Jr., L. C., et al. 2008, *ArXiv e-prints*, 805

Table 1 Ambient conditions at the zenith and in the visible during the observations

Filter	date [UT]	airmass	seeing ["]	τ_0 [ms]
K _s	2007-11-25 06:33	1.09	1'90±0'13	0.9±0.1
H	2007-12-01 07:37	1.23	0'63±0'05	3.2±0.3

Table 2 Instrumental zeropoints for the MAD observations

Method	Filter	Zeropoint [mag]
Aperture	H	25.25±0.07
Aperture	K _s	24.62±0.10
PSF	H	25.30±0.07
PSF	K _s	24.56±0.10

van Loon, J. T. & Oliveira, J. M. 2003, *A&A*, 405, L33

Walborn, N. R. 1974, *ApJ*, 191, L95+

Zapatero Osorio, M. R., Béjar, V. J. S., Bihain, G., et al. 2008, *A&A*, 477, 895

Zapatero Osorio, M. R., Béjar, V. J. S., Martín, E. L., et al. 2000, *Science*, 290, 103

Zapatero Osorio, M. R., Béjar, V. J. S., Martín, E. L., et al. 2002, *ApJ*, 578, 536

Zapatero Osorio, M. R., Caballero, J. A., Béjar, V. J. S., et al. 2007, *A&A*, 472, L9

Table 3 Catalog of sources detected in the MAD images

Name	RA (J2000)	Dec (J2000)	H [mag]	K _s [mag]	Other name	Comment
<i>SigOri-MAD-1</i>	05:38:43.5	-02:36:23.7	14.95±0.07	14.59±0.14		Spitzer, 0.050 M _⊙
SigOri-MAD-2	05:38:43.9	-02:36:01.5	17.99±0.09	17.57±0.20		
SigOri-MAD-3	05:38:44.1	-02:36:06.3	...	9.01±0.10	σ Ori C, Mayrit 11238	Spitzer
<i>SigOri-MAD-4</i>	05:38:44.1	-02:36:04.4	14.63±0.07	14.07±0.10		
SigOri-MAD-5	05:38:44.2	-02:36:12.7	20.81±0.07	<19.0		No SofI
<i>SigOri-MAD-6</i>	05:38:44.5	-02:35:35.0	16.11±0.07	15.77±0.14	2MASS J05384454-0235349	Spitzer, 0.025 M _⊙
SigOri-MAD-7	05:38:44.6	-02:36:18.7	18.99±0.12	18.19±0.18		
SigOri-MAD-8	05:38:44.8	-02:35:56.9	12.84±0.07	12.65±0.07	σ Ori IRS1 B	NACO
SigOri-MAD-9	05:38:44.8	-02:35:57.1	10.70±0.07	10.48±0.01	σ Ori IRS1 A	NACO
SigOri-MAD-10	05:38:45.0	-02:36:15.4	21.65±0.57	<19.0		No SofI
SigOri-MAD-11	05:38:45.2	-02:35:57.7	19.29±0.53	18.31±0.32		No SofI/ NACO
SigOri-MAD-12	05:38:45.2	-02:35:44.0	18.21±0.08	17.57±0.17		
SigOri-MAD-13	05:38:45.2	-02:35:51.5	18.54±0.10	17.19±0.17		No SofI/No NACO
SigOri-MAD-14	05:38:45.2	-02:35:41.2	13.19±0.07	12.70±0.14	Mayrit 21023	Spitzer
<i>SigOri-MAD-15</i>	05:38:45.6	-02:35:29.3	16.15±0.07	15.72±0.14		Spitzer, 0.025 M _⊙
SigOri-MAD-16	05:38:45.7	-02:35:38.4	19.39±0.12	19.20±0.26		
SigOri-MAD-17	05:38:45.7	-02:35:23.7	19.23±0.12	18.56±0.15		
SigOri-MAD-18	05:38:45.8	-02:36:13.5	18.26±0.09	17.77±0.19		
SigOri-MAD-19	05:38:45.9	-02:35:26.7	17.38±0.08	17.03±0.16		
SigOri-MAD-20	05:38:46.0	-02:35:57.1	18.53±0.10	18.16±0.16		
SigOri-MAD-21	05:38:46.4	-02:35:49.7	20.07±0.17	<19.0		No SofI
SigOri-MAD-22	05:38:46.4	-02:36:00.7	19.25±0.12	18.80±0.28		
<i>SigOri-MAD-23</i>	05:38:46.5	-02:35:48.3	14.50±0.07	14.11±0.14	2MASS J05384652-0235479	Spitzer, 0.060 M _⊙
SigOri-MAD-24	05:38:46.7	-02:36:18.3	18.75±0.10	18.05±0.21		
<i>SigOri-MAD-25</i>	05:38:46.8	-02:36:24.1	15.72±0.07	15.37±0.14		Spitzer, 0.030 M _⊙
SigOri-MAD-26	05:38:46.8	-02:36:06.2	20.97±0.27	18.88±0.15		
SigOri-MAD-27	05:38:47.0	-02:35:58.7	18.32±0.09	18.26±0.16		H-band uncertain
SigOri-MAD-28	05:38:47.1	-02:35:53.8	19.25±0.11	18.97±0.33		
SigOri-MAD-29	05:38:47.1	-02:35:51.9	19.55±0.13	19.12±0.25		
SigOri-MAD-30	05:38:47.1	-02:36:05.6	21.39±0.44	<19.0		No SofI
SigOri-MAD-31	05:38:47.2	-02:36:05.4	17.83±0.08	17.04±0.16		Spitzer, 7 M _{Jup}
SigOri-MAD-32	05:38:47.2	-02:35:50.5	21.01±0.07	<19.5		No SofI
SigOri-MAD-33	05:38:47.3	-02:36:00.8	19.75±0.15	18.60±0.15		
SigOri-MAD-34	05:38:47.4	-02:35:25.2	11.05±0.07	10.42±0.14	Mayrit 53049	Spitzer
SigOri-MAD-35	05:38:48.0	-02:35:52.4	17.63±0.08	17.14±0.17		
SigOri-MAD-36	05:38:48.1	-02:35:51.0	16.72±0.07	16.30±0.15		

Note – Objects with H-band luminosity corresponding to a PMO (defined here as $M \leq 0.012 M_{\odot}$) are indicated in bold face. Objects with H-band luminosity corresponding to a BD (defined here as $0.012 < M \leq 0.072 M_{\odot}$) are indicated in italic. The errors include the zeropoint uncertainties.

Table 4 Log of Spitzer observations

Program ID	P.I.	Date Obs. [DD-MM-YYYY]	Exposure time [s]	Number of frames
37	Fazio	08-10-2004	1.2/30	270/270
30395	Scholz	03-04-2007	100	24

Table 5 Spitzer IRAC photometry of sources detected in the MAD images

Name	3.6 μm [mJy]	4.5 μm [mJy]	5.8 μm [mJy]	8.0 μm [mJy]
SigOri-MAD-1	0.46±0.04	0.22±0.09	0.10±0.04	0.11±0.05
SigOri-MAD-3	54.6±0.04	43.0±0.04	20.9±0.5	13.19±0.7
SigOri-MAD-6	0.22±0.17
SigOri-MAD-14	2.19±0.10	1.49±0.30	1.60±0.30	...
SigOri-MAD-15	0.17±0.08	0.10±0.02
SigOri-MAD-23	0.68±0.06	...	0.3±0.1	...
SigOri-MAD-25	0.18±0.04	0.27±0.05
SigOri-MAD-31	0.09±0.03
SigOri-MAD-34	21.2±0.4	16.3±0.5	15.1±0.6	19.1±0.7

Table 6 Spitzer IRAC photometry of the two L-dwarf candidates detected in the SofI images

Name	3.6 μm [mJy]	4.5 μm [mJy]	5.8 μm [mJy]	8.0 μm [mJy]	other name
SigOri-SofI-142	0.073±0.010	0.070±0.010	0.045±0.007	...	Mayrit 111335
SigOri-SofI-181	0.080±0.012	0.067±0.010	0.041±0.010	...	Mayrit 72345

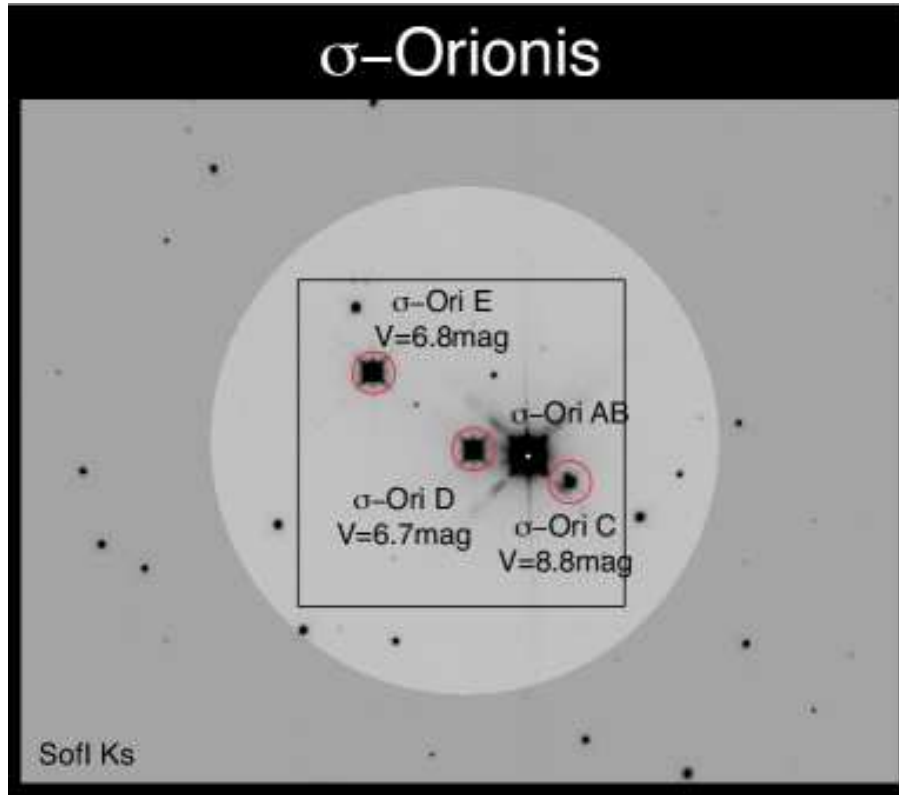


Fig. 1 NTT/SOFI K_s -band mosaic image of the observed field. The field of view within which the wavefront sensing stars for MAD can be selected is represented with a circle of $2'$ diameter. The 3 wavefront sensing reference stars are indicated with red circles and their names and V-band luminosities overplotted. The 1.5×1.5 field-of-view of the final images is also represented. North is up and east is left.

Table 7 Relative astrometry and photometry of the multiple systems

System	date UT [YYYY-MM-DD HH:MM]	Separation [mas]	P.A. [$^\circ$]	ΔH [mag]	ΔK_s [mag]	Instrument
σ -Ori AB	2004-10-11 09:44	255.7 ± 1.8	100.9 ± 0.4	NACO
σ -Ori AD	2004-10-11 09:44	13037.2 ± 27	84.1 ± 0.4	NACO
σ -Ori IRS1 AB	2004-10-11 09:44	236.3 ± 2.4	318.1 ± 0.4	...	2.19 ± 0.01	NACO
σ -Ori IRS1 AB	2007-12-01T07:23	242.9 ± 3.6	317.0 ± 0.7	2.13 ± 0.10	2.17 ± 0.07	MAD
σ -Ori Cab	2007-12-01T07:23	1991.5 ± 3.9	11.5 ± 0.7	5.50 ± 0.07	5.05 ± 0.14	MAD
σ -Ori Eab	2007-12-01T07:23	≈ 330	≈ 391	MAD

Note – In addition to the uncertainties on the measurement, these values include errors related to the camera distortions (of the order of 1% of the pixel scale for NACO, see e.g. Seifahrt et al., 2007; Eggenberger et al., 2007, not calibrated but assumed to be of the same order for MAD).

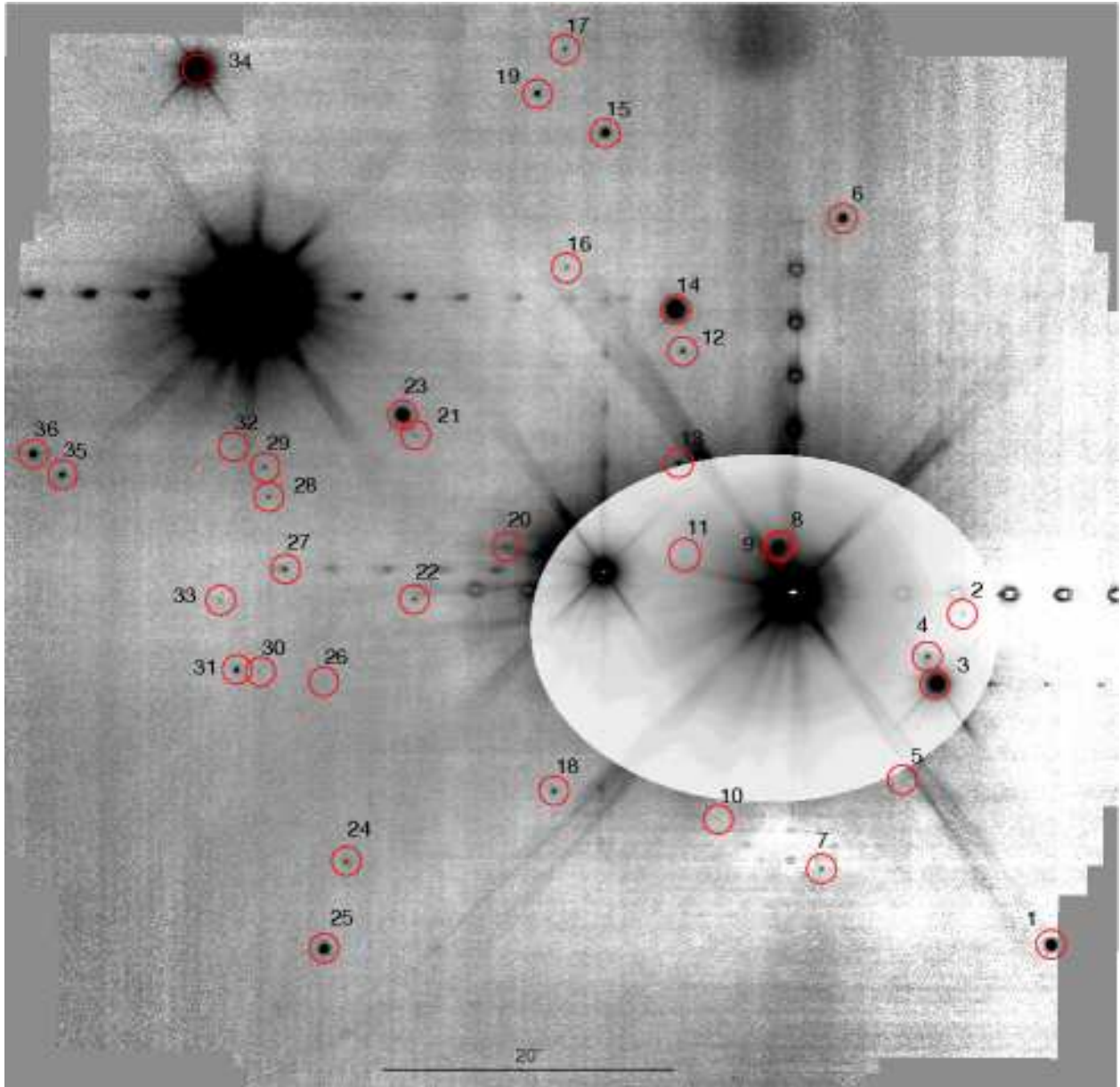


Fig. 2 MAD H-band mosaic image with all the detected sources overplotted. The levels have been stretched differently close to the bright OB stars to enhance the contrast. The source number are indicated (see Table 3). North is up and east is left and the scale is indicated.

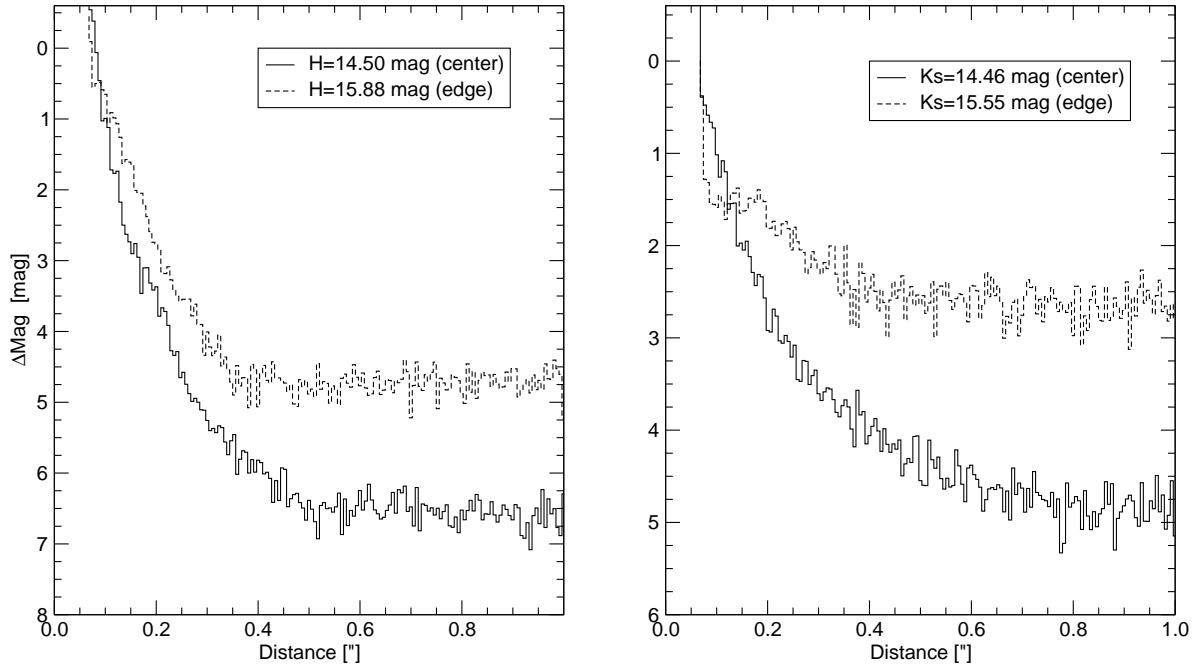


Fig. 3 Limit of sensitivity in the H-band (left panel) and K-band (right panel) for 2 different stars located in a region of good AO correction (center) and worse AO correction (edge). The curve have been computed from the $3\text{-}\sigma$ noise of the radial profile of the PSF.

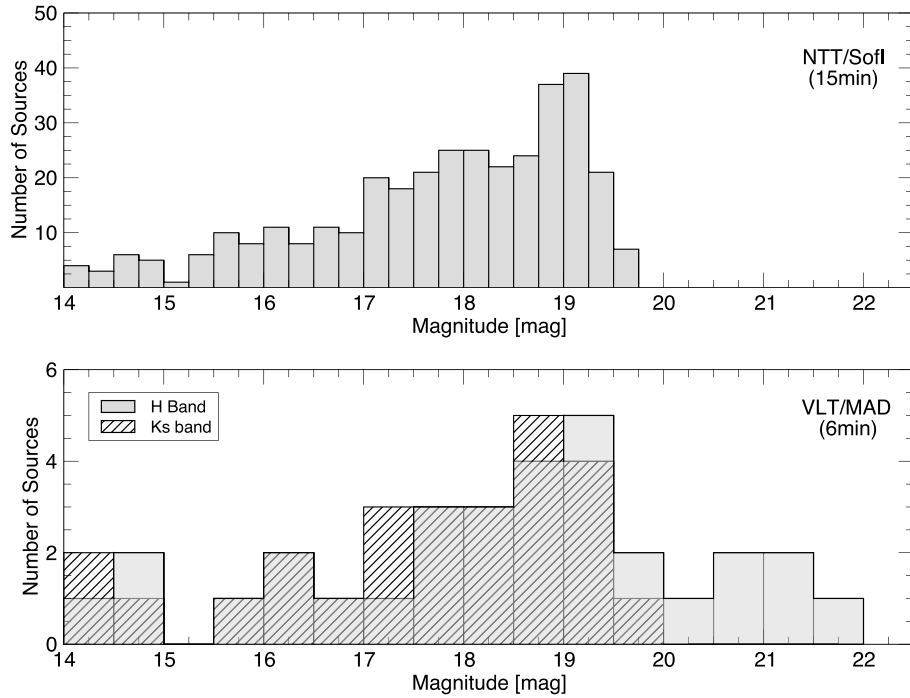


Fig. 4 Distribution of magnitude of the sources detected in the SofI (15 min on-source exposure) and MAD (6 min on-source exposure) images. The limits of completeness in the MAD images reach $K_s \approx 19.5 \text{ mag}$ and $H \approx 20.0 \text{ mag}$. It is not homogeneous over the entire image, as large areas are contaminated by the strong halos of the bright massive stars.

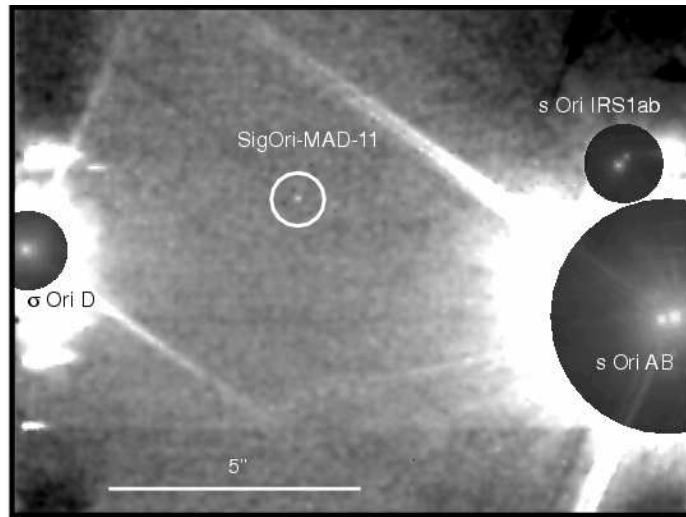


Fig. 5 NACO K_s image of σ Ori AB, D and IRS1. The image was wavelet filtered to enhance SigOri-MAD-11 detection, indicated with a white circle. East is left and north is up and the scale is shown. The contrast have been stretched differently around the bright OB stars to increase the dynamic of the figure.

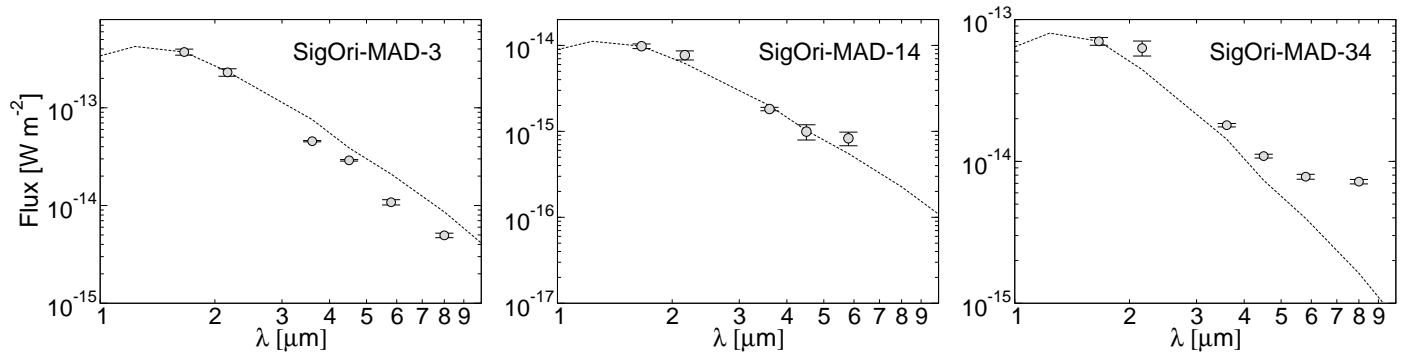


Fig. 6 Spectral energy distributions of the MAD stellar sources with *Spitzer* IRAC counterparts. The dashed line represent the median SED of confirmed members without excess as derived by Hernández et al. (2007) and normalized to the same H-band flux as the MAD source. SigOri-MAD-34 display some mid-IR excess indicating the presence of circumstellar material.

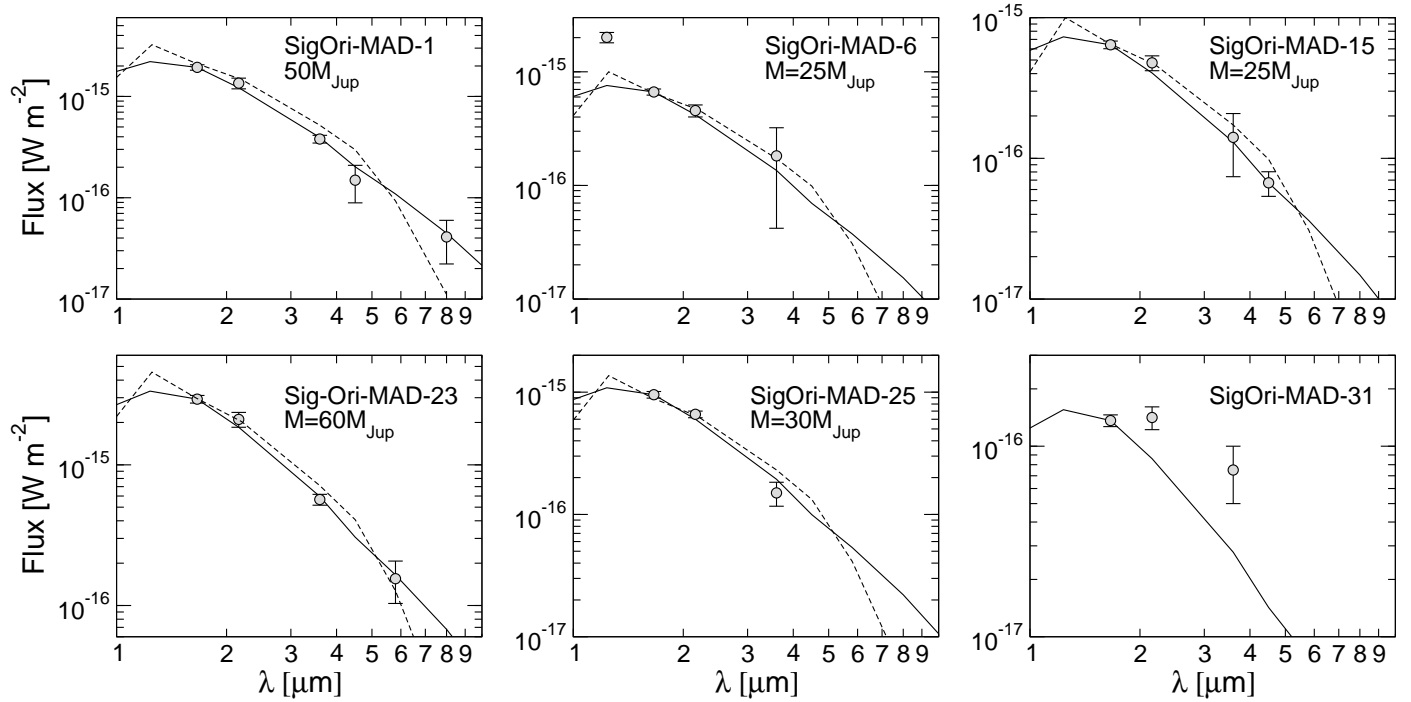


Fig. 7 Spectral energy distributions of the MAD substellar candidates with *Spitzer* IRAC counterparts. The plain line represent the median SED of confirmed members without excess as derived by Hernández et al. (2007) and normalized to the same H-band flux as the MAD source. The 1 Myr synthetic DUSTY SEDs for the given H-band luminosities and at a distance of 440 pc are overplotted with a dashed line and the corresponding masses indicated. The good match suggest that the sources are indeed members of the association.

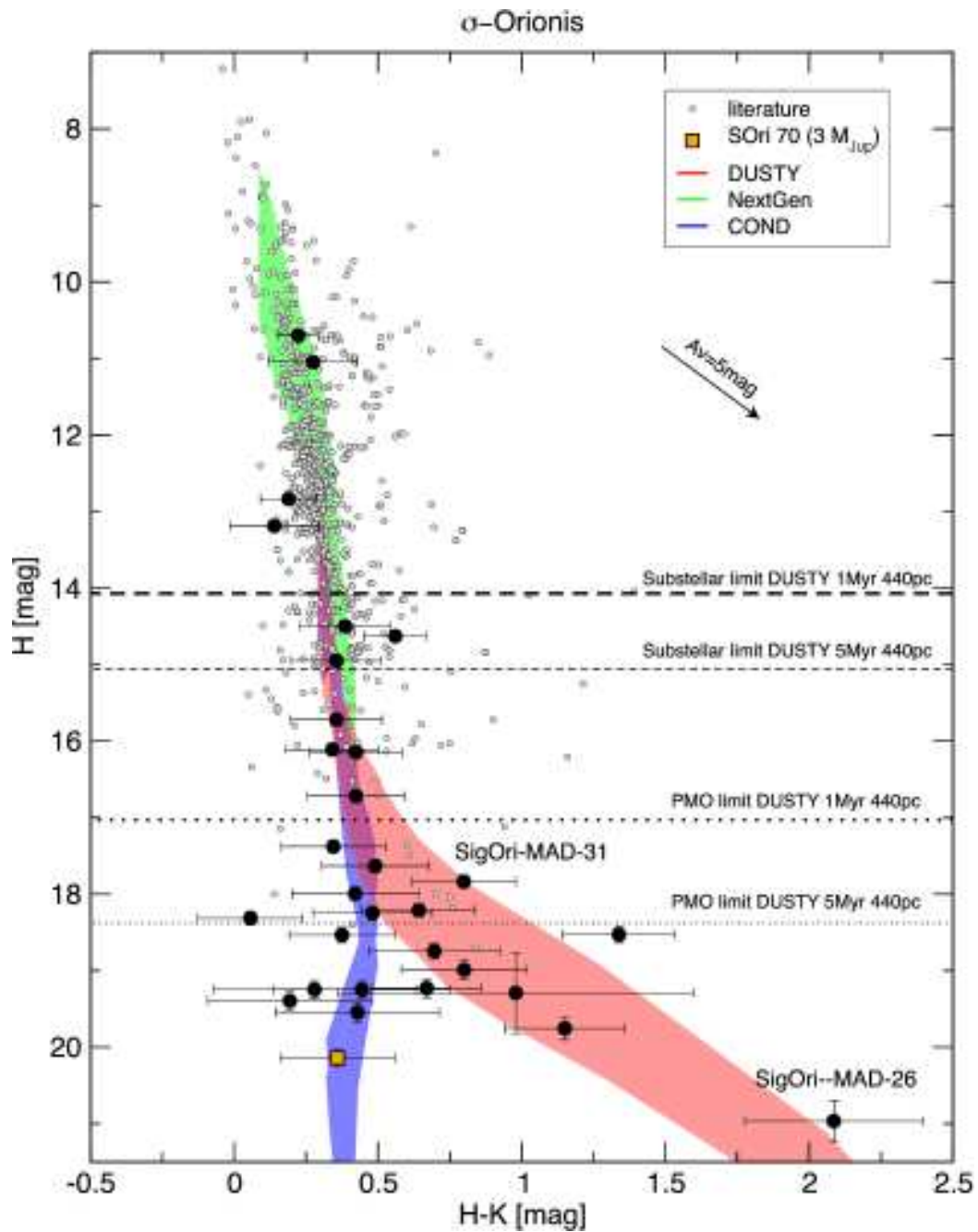


Fig. 8 H vs H-K color-magnitude diagram of the σ -Orionis cluster. The MAD measurements are represented by black circles. The DUSTY, NextGen and COND isochrones between 1–5 Myr and 350–440 pc are represented in red, green and blue shaded areas, respectively. Measurements for cluster members from the literature are overplotted as grey circles (Caballero, 2008c; Caballero et al., 2007; Scholz & Eislöffel, 2004; Béjar et al., 2004; Sherry et al., 2004). The confirmed PMO S Ori 70 (Zapatero Osorio et al., 2008) is represented with an orange square. The substellar and deuterium burning limit from the DUSTY models for 1 Myr and 5 Myr at a distance of 440 pc as well as a $A_V=5$ mag reddening vector are represented.

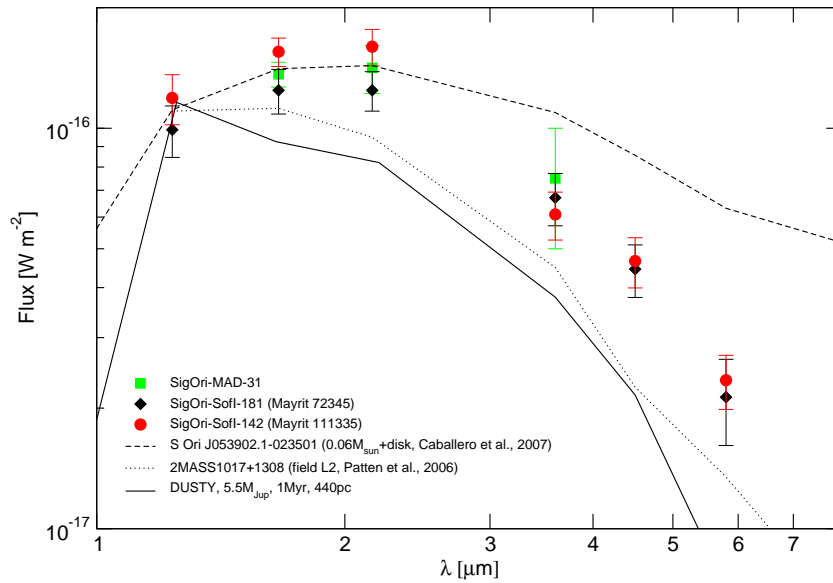


Fig. 9 Spectral energy distributions of the substellar candidates with SofI and *Spitzer* IRAC counterparts (SigOri-Sofi-181, black diamonds, and SigOri-Sofi-142, red dots), as well as SigOri-MAD-31 (green squares). The line represents the 1 Myr DUSTY SED of a $\approx 5.5 M_{\text{Jup}}$ object at a distance of 440 pc. The dotted line represents the SED of the field L2 dwarf 2MASS J1017+1308 (Patten et al., 2006) normalized to the average J-band fluxes of the two candidates. The dashed line represents the SED of the 0.060 brown dwarf with a disk S Ori J053902.1-023501 as reported by Caballero et al. (2007) and normalized to the average J-band fluxes of the two candidates. The three L-dwarf candidates display a clear mid-IR excess when compared to the field L2 dwarf or the DUSTY photospheric model. Their SED look like lower luminosity analogues of the substellar member S Ori J053902.1-023501 (Caballero et al., 2007).

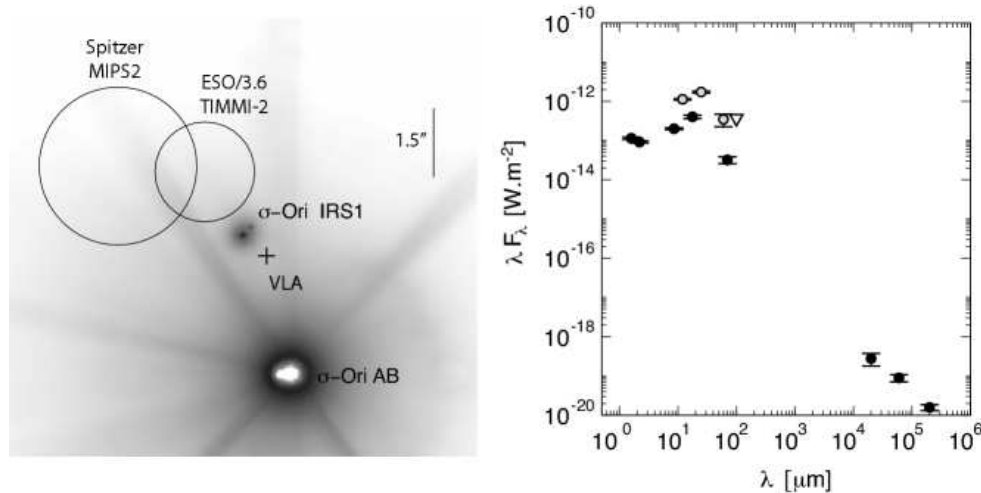


Fig. 10 Left panel: MAD H-band image around σ Ori IRS1. The *Spitzer* 70 μm , VLA (Drake, 1990) and TIMMI-2 (van Loon & Oliveira, 2003) detections are overplotted with circles. The size of the circle corresponds to the FWHM of the source in these images, except for the VLA detection which has a much better accuracy ($< 0''.1$) and is represented with a dimensionless cross. The different positions have been aligned using the MAD H-band image as reference frame. The uncertainty on the MAD mosaic image astrometric solution is $\approx 0''.1$. All these detections are closer to σ Ori IRS1 than to σ Ori AB. The scale is indicated. North is up and east is left. Right Panel: Spectral energy distribution of σ Ori IRS1. The IRAS fluxes are represented with grey circles (detections) or a triangle (upper limit). As the source is unresolved in the TIMMI-2, *Spitzer* and VLA images, the H and K_s fluxes correspond to the combined fluxes of the two components as measured in the MAD and NACO images.

Table 8 NTT/SofI Ks-band photometry

Name	RA (J2000)	Dec (J2000)	Ks [mag]	Nearest 2MASS	Nearest Mayrit
SigOri-SofI-1	05:38:33.3	-02:36:17.0	13.05	05383335-0236176	
SigOri-SofI-2	05:38:33.3	-02:36:17.1	10.99	05383335-0236176	
SigOri-SofI-3	05:38:33.3	-02:36:44.2	18.02		
SigOri-SofI-4	05:38:33.5	-02:34:53.1	18.81		
SigOri-SofI-5	05:38:33.5	-02:35:40.6	18.17		
SigOri-SofI-6	05:38:33.5	-02:36:05.0	18.84		
SigOri-SofI-7	05:38:33.6	-02:35:00.3	17.38		
SigOri-SofI-8	05:38:33.7	-02:36:47.5	14.71	05383376-0236479	
SigOri-SofI-9	05:38:33.7	-02:36:57.6	17.60		
SigOri-SofI-10	05:38:33.7	-02:36:58.3	18.88		
SigOri-SofI-11	05:38:33.9	-02:35:31.0	18.44		
SigOri-SofI-12	05:38:33.9	-02:36:26.3	19.16		
SigOri-SofI-13	05:38:34.0	-02:36:36.9	13.68	05383405-0236375	165257
SigOri-SofI-14	05:38:34.0	-02:36:37.0	10.95	05383405-0236375	165257
SigOri-SofI-15	05:38:34.2	-02:34:49.8	19.52		
SigOri-SofI-16	05:38:34.6	-02:38:26.1	16.88		
SigOri-SofI-17	05:38:34.8	-02:34:27.3	17.35		
SigOri-SofI-18	05:38:34.8	-02:36:20.0	16.59	05383491-0236206	
SigOri-SofI-19	05:38:34.9	-02:36:20.1	14.12	05383491-0236206	
SigOri-SofI-20	05:38:35.0	-02:34:55.5	17.97	05383510-0234559	
SigOri-SofI-21	05:38:35.1	-02:34:55.9	16.48	05383510-0234559	
SigOri-SofI-22	05:38:35.1	-02:35:57.8	18.25		
SigOri-SofI-23	05:38:35.2	-02:34:09.2	19.54		
SigOri-SofI-24	05:38:35.2	-02:34:21.4	18.72		
SigOri-SofI-25	05:38:35.2	-02:34:36.8	17.69		
SigOri-SofI-26	05:38:35.2	-02:34:37.4	16.58		
SigOri-SofI-27	05:38:35.2	-02:34:51.9	18.09		
SigOri-SofI-28	05:38:35.3	-02:36:02.1	17.01		
SigOri-SofI-29	05:38:35.3	-02:38:37.1	17.42	05383540-0238373	
SigOri-SofI-30	05:38:35.4	-02:35:47.1	16.80		
SigOri-SofI-31	05:38:35.4	-02:38:37.0	14.95	05383540-0238373	
SigOri-SofI-32	05:38:35.5	-02:35:34.4	18.93		
SigOri-SofI-33	05:38:35.6	-02:34:26.1	18.32		
SigOri-SofI-34	05:38:35.7	-02:34:26.8	17.07		
SigOri-SofI-35	05:38:35.9	-02:35:01.7	19.08		
SigOri-SofI-36	05:38:36.0	-02:38:08.9	16.08		
SigOri-SofI-37	05:38:36.1	-02:34:27.0	18.91		
SigOri-SofI-38	05:38:36.3	-02:36:28.2	18.45		
SigOri-SofI-39	05:38:36.4	-02:37:32.1	16.22		
SigOri-SofI-40	05:38:36.5	-02:33:19.7	18.81		
SigOri-SofI-41	05:38:36.5	-02:35:33.4	18.75		
SigOri-SofI-42	05:38:36.7	-02:33:22.7	19.14		
SigOri-SofI-43	05:38:36.7	-02:34:57.1	18.81		
SigOri-SofI-44	05:38:36.8	-02:35:16.0	12.70	05383686-0235163	
SigOri-SofI-45	05:38:36.8	-02:36:42.8	12.00	05383687-0236432	126250
SigOri-SofI-46	05:38:37.0	-02:35:15.1	15.51	05383686-0235163	
SigOri-SofI-47	05:38:37.1	-02:37:02.7	17.06	05383721-0237031	
SigOri-SofI-48	05:38:37.1	-02:37:05.8	19.21		
SigOri-SofI-49	05:38:37.2	-02:35:31.8	17.86		
SigOri-SofI-50	05:38:37.2	-02:36:24.7	17.78		
SigOri-SofI-51	05:38:37.2	-02:37:02.7	13.78	05383721-0237031	
SigOri-SofI-52	05:38:37.3	-02:33:52.7	19.20		
SigOri-SofI-53	05:38:37.3	-02:36:10.2	19.27		
SigOri-SofI-54	05:38:37.3	-02:37:16.1	18.57		
SigOri-SofI-55	05:38:37.5	-02:37:34.0	18.55		
SigOri-SofI-56	05:38:37.6	-02:34:31.5	17.40		
SigOri-SofI-57	05:38:37.6	-02:36:52.0	20.21	05383764-0236523	
SigOri-SofI-58	05:38:37.7	-02:36:00.2	17.41		
SigOri-SofI-59	05:38:37.8	-02:33:32.8	17.60		
SigOri-SofI-60	05:38:37.8	-02:34:33.2	18.77		
SigOri-SofI-61	05:38:37.8	-02:35:06.6	17.03		
SigOri-SofI-62	05:38:37.8	-02:35:48.7	18.63		
SigOri-SofI-63	05:38:37.9	-02:37:27.6	16.64		
SigOri-SofI-64	05:38:38.0	-02:34:48.0	18.35		
SigOri-SofI-65	05:38:38.1	-02:35:07.3	19.20		
SigOri-SofI-66	05:38:38.1	-02:35:41.6	15.45	05383808-0235418	
SigOri-SofI-67	05:38:38.1	-02:35:51.5	17.85		
SigOri-SofI-68	05:38:38.1	-02:36:09.6	15.51	05383814-0236099	
SigOri-SofI-69	05:38:38.2	-02:36:30.0	15.52	05383823-0236306	
SigOri-SofI-70	05:38:38.2	-02:36:38.0	10.20	05383822-0236384	105249
SigOri-SofI-71	05:38:38.2	-02:38:24.5	18.84		

This figure "mad_H.png" is available in "png" format from:

<http://arxiv.org/ps/0808.3890v1>